JM PAPERS

Evidence for the incompatibility of smoothed particle hydrodynamics and eddy viscosity models for large eddy simulations

Max Okraschevski[1,2] , Niklas Bürkle[1], Markus Wicker[1], Rainer Koch[1] and Hans-Joerg Bauer[1]

[1]Institute of Thermal Turbomachinery, Karlsruhe Institute of Technology, Kaiserstraße 12, 76131 Karlsruhe, Germany

[2]Institute of Engineering Thermodynamics, German Aerospace Center, 89081 Ulm, Germany; Helmholtz Institute Ulm for Electrochemical Energy Storage, 89081 Ulm

Corresponding author: Max Okraschevski, max.okraschevski@dlr.de

In this work, we will present evidence for the incompatibility of smoothed particle hydrodynamics (SPH) methods and eddy viscosity models. Taking a coarse-graining perspective, we physically argue that SPH methods operate intrinsically as Lagrangian large eddy simulations for turbulent flows with strongly overlapping discretisation elements. However, these overlapping elements in combination with numerical errors cause a significant amount of implicit subfilter stresses (SFS). Considering a Taylor–Green flow at $Re = 10^4$, the SFS will be shown to be relevant where turbulent fluctuations are created, explaining why turbulent flows are challenging even for current SPH methods. Although one might hope to mitigate the implicit SFS using eddy viscosity models, we show a degradation of the turbulent transition process, which is rooted in the non-locality of these methods.

Key words: turbulence simulation, homogeneous turbulence, turbulence theory

1. Introduction

The smoothed particle hydrodynamics (SPH) method was proposed in 1977 as a Lagrangian discretisation method for fluid dynamics (Gingold & Monaghan 1977; Lucy 1977) and matured significantly since then, as detailed in several reviews (Springel 2010; Monaghan 2012; Price 2012; Shadloo, Oger & Touze 2016; Ye *et al.* 2019; Lind, Rogers & Stansby 2020; Sigalotti, Klapp & Gesteira 2021). Originally, the SPH method featured
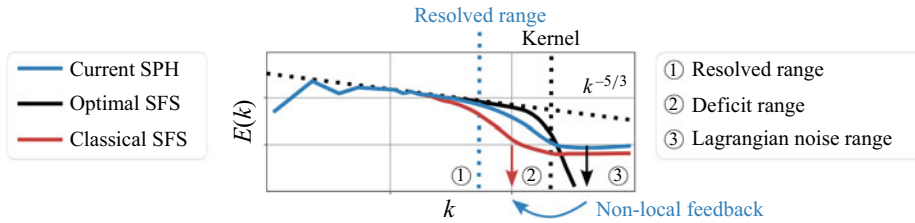
Figure 1. Typical distribution of spectral energy density obtained with SPH methods for incompressible turbulence. The properly resolved range with large eddies passes into an energy deficit range that is non-locally caused and followed by a Lagrangian noise range. From an optimal SFS model, we would expect a reduction of the Lagrangian noise in favour of the deficit range. However, with incompatible classical SFS models, the noise is barely reduced and the deficit range is exacerbated due to non-locality.

serious numerical convergence problems due to the fact that the consistency of spatial derivative operators is strongly affected by the local particle arrangement, which only can be compensated by a drastic increase in the number of neighbour particles N_{ngb} (Zhu, Hernquist & Li 2015). This is especially problematic in strong shear flows and subsonic turbulence, resulting in zeroth-order errors related to excessive numerical dissipation for small N_{ngb} (Ellero, Español & Adams 2010; Bauer & Springel 2012; Colagrossi *et al.* 2013; Hopkins 2015).

Pioneered by the work of Vila (1999), current SPH methods, as recently compared by Eirís *et al.* (2023), mostly eliminated this convergence issue by the use of at least one of the following two strategies:

(i) a consistent approximation of spatial derivatives by either a reproducing kernel (RK) or moving least squares (MLS) approach (Hopkins 2015; Frontiere, Raskin & Owen 2017)

(ii) an arbitrary Lagrangian–Eulerian (ALE) formulation with transport velocity as noise mitigation technique (Oger *et al.* 2016; Antuono *et al.* 2021*b*), also rigorously incorporating particle shifting (Xu, Stansby & Laurence 2009; Lind *et al.* 2012).

In line with these positive developments, the confidence in the ability of current SPH methods to capture incompressible turbulence increases. Especially in complex multiphase flow situations, where SPH can play to its strengths, these methods are nowadays optimistically combined with a large eddy simulation (LES) perspective (Colagrossi *et al.* 2021; Lai *et al.* 2022; King *et al.* 2023; Meringolo *et al.* 2023). In the following, we will refer to this combination of SPH methods with LES simply as SPH-LES for brevity. As already mentioned by Bicknell (1991), such a confluence is intuitive since the SPH kernel and the LES low-pass filter, building the foundation of both methods, are mathematically congruent. Certainly, the development of rigorous combined SPH-LES theories is a very recent topic; e.g. Di Mascio *et al.* (2017), Antuono *et al.* (2021*a*), Okraschevski *et al.* (2022).

One central remaining issue is that all these current SPH-LES studies intuitively model one of the central LES objects, namely the subfilter stress (SFS) tensor $\boldsymbol{\tau}_{SFS}$, by classical, functional eddy viscosity approaches, employing the Boussinesq hypothesis (Schmitt 2007). In Okraschevski *et al.* (2022), we could argue that for classical SPH, physically reinterpreting this method from a spatial coarse-graining perspective, eddy viscosity modelling must fail due to the non-locality of the SPH method (Du & Tian 2020; Vignjevic, DeVuyst & Campbell 2021; Yao, Zhou & Qian 2022). The resulting incompatibility is illustrated in figure 1 and manifests in a spectral mismatch where the classical SFS model is introduced. Yet one might object that this is just

a consequence of the classical SPH approach considered in our former study. This is where the following work comes into play showing that our coarse-graining perspective generally applies to current SPH methods. (The aforementioned convergence issues with SPH, the countermeasures listed above and the subsequent rationale strictly apply only to Lagrangian SPH methods, inherently including particle disorder. For regular particle distributions in an Eulerian frame, the convergence issues to begin with can be fully eliminated (Hopkins 2015; Lind & Stansby 2016) with proper numerical schemes (Appendix A), and accordingly, the spectral peculiarities in figure 1. However, since we believe that the Lagrangian character is still a key argument for current SPH methods, we will subsequently focus on this specific reference frame.) Hence classical eddy viscosity modelling, as already indicated by Rennehan (2021), is compromising the most accurate prediction of turbulence possible, and necessitates the development of completely new and specific SFS models in the SPH-LES context. This perspective could accentuate even more the advantages of current SPH methods over traditional grid-based approaches in application areas such as multiphase flows encompassing turbulence.

However, should such an improved SFS model not be available soon, we definitively advise operating current SPH methods for aforementioned flows using no explicit SFS model. Thus we will broadly argue in favour of the notion that current Lagrangian SPH methods operate intrinsically as implicit LES. The latter is an established concept in the grid-based community, and relies on properly designed discretisation errors to provide an implicit SFS contribution; e.g. Grinstein, Margolin & Rider (2007), Dairay *et al.* (2017), Moura *et al.* (2017), Fehn *et al.* (2022), Volpiani (2024). Heuristically, it seems that these implicit SFS in SPH methods emerge from statistical physics principles (Posch, Hoover & Kum 1995; Ellero *et al.* 2010; Borreguero *et al.* 2019; Okraschevski *et al.* 2021*a*), which we will confirm in more detail below using Hardy's theory (Hardy 1982).

2. Novelty and implications

In our former works (Okraschevski *et al.* 2021*a*,*b*) we laid the theoretical foundation to be summarised in §3 with Hardy's theory (Hardy 1982) at its core. Based on this, we could demonstrate that SPH-LES with classical SPH seems fundamentally incompatible with explicit viscosity models due to the non-local characteristic of the discretisation (Okraschevski *et al.* 2022; Okraschevski 2024). Here, we report evidence for the first time that this incompatibility also holds for SPH-LES with current SPH methods, which are not plagued by the classical SPH problems as described in §1. As a consequence, we believe that classical eddy viscosity models for the SFS tensor τ_{SFS} are detrimental in SPH-LES of incompressible turbulence, and that novel models matching the discretisation characteristics must be developed. This insight will particularly improve the predictive power of current SPH methods in complex multiphase flows, when incompressible turbulence is an inevitable aspect of the considered flow.

3. Coarse-graining perspective on SPH methods

Although current SPH methods might not suffer from the same convergence issue as their original ancestor, at their heart they still employ quasi-Lagrangian particles. (This term is usually used within ALE frameworks (Vogelsberger *et al.* 2012; Oger *et al.* 2016; Antuono *et al.* 2021*a*). Here, we also include pseudo-Lagrangian particles (Vogelsberger *et al.* 2012) – also called purely Lagrangian particles in other works (Oger *et al.* 2016; Antuono *et al.* 2021*a*) – in the definition.) These are connected by a spherical, positive and monotonously decaying kernel $W : \mathbb{R}^3 \to \mathbb{R}$ with compact support $V_{\boldsymbol{x}}$, being centred
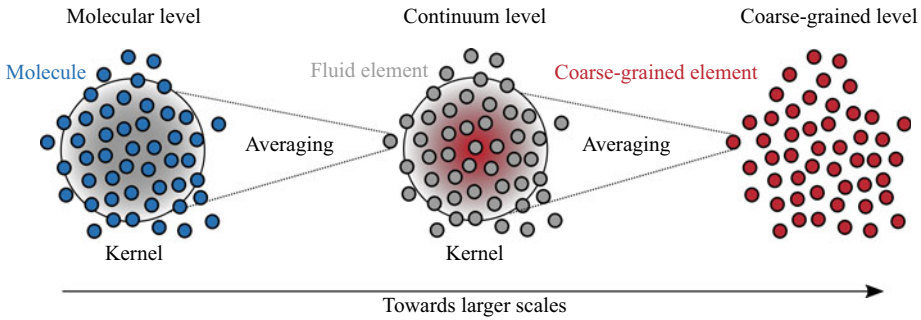
Figure 2. Illustration of spatial coarse-graining emerging from the generalisation of Hardy's theory (Hardy 1982; Okraschevski *et al.* 2021*b*). Adapted from Okraschevski *et al.* (2022).

at the quasi-Lagrangian particles $x \in \mathbb{R}^3$. Hence even current SPH methods intrinsically contain two resolution scales, namely the mean particle distance Δl, and the larger kernel diameter D_K. We termed this property particle duality in our former work (Okraschevski *et al.* 2022). This is a characteristic peculiarity compared to grid-based discretisation techniques, and results in strongly overlapping discretisation elements, i.e. a non-local discretisation. Despite the fact that numerical convergence in current SPH methods can be reached using a constant ratio $D_K / \Delta l = O(1)$ (Vila 1999; Hopkins 2015) resulting in a fixed number of neighbours N_{ngb} inside the kernel, one still might wonder which flow scales can be effectively resolved. Taking a conservative point of view, it must be expected that flow scales can be captured maximally up to the kernel diameter D_K. By means of such a rationale, one implicitly interprets SPH methods from a spatial coarse-graining perspective at the effective scale D_K. Such a coarse-graining perspective is not only a convenient footing in the following, but also the physical foundation of the LES community (Eyink & Drivas 2018), and even more so a general perspective employed by fluid dynamicists (Irving & Kirkwood 1950; Okraschevski *et al.* 2021*b*; Eyink 2024). In the LES community, the coarse-graining is also synonymously called the filtering approach (Germano 1992). Although the different terminologies describe equivalent mathematical operations, we believe that the term coarse-graining raises the awareness for a geometric interpretation in terms of a hierarchical clustering of Lagrangian particles (figure 2). The aforementioned can be vividly unravelled by generalising the theory of Hardy from statistical physics (Hardy 1982; Okraschevski *et al.* 2021*b*), and highlights the conceptual similarity to the Lagrangian discretisation techniques of interest. Hence we anticipate that SPH methods aim to solve an effective field equation and intrinsically operate as Lagrangian LES. By defining the Lagrangian derivative as

$$\frac{\mathrm{d}}{\mathrm{d}t} := \partial_t + \tilde{v} \cdot \nabla_x \tag{3.1}$$

and the spatial coarse-graining of a scalar field $f : \mathbb{R}^3 \times \mathbb{R}_0^+ \to \mathbb{R}$ over V_x as

$$\overline{f}(x, t) = \int_{V_x} f(y, t) \, W(x - y) \, \mathrm{d}y, \tag{3.2}$$

we will subsequently consider barotropic flows in a Lagrangian reference frame

$$\frac{\mathrm{d}\overline{\rho}}{\mathrm{d}t}(x, t) = -\overline{\rho}(x, t) \, \nabla_x \cdot \tilde{v}(x, t), \tag{3.3}$$
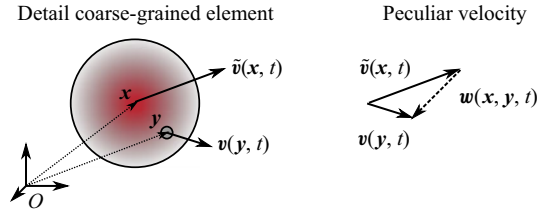
Figure 3. Visualisation of the velocity decomposition in (3.8). Adapted from Okraschevski (2024).

$$\overline{\rho}(\boldsymbol{x}, t)\frac{\mathrm{d}\tilde{\boldsymbol{v}}}{\mathrm{d}t}(\boldsymbol{x}, t) = -\boldsymbol{\nabla}_{\boldsymbol{x}}\overline{p}(\boldsymbol{x}, t) + \mathrm{div}_{\boldsymbol{x}}\left[\tilde{\boldsymbol{\tau}}_{visc} + \boldsymbol{\tau}_{SFS}\right](\boldsymbol{x}, t), \tag{3.4}$$

$$\overline{p}(\boldsymbol{x}, t) = \overline{p}_{ref} + c_s^2(\overline{\rho}(\boldsymbol{x}, t) - \overline{\rho}_{ref}). \tag{3.5}$$

Moreover, we will assume for (3.3), (3.4) and (3.5) a weakly compressible, low Mach number flow ($Ma < 0.3$). Hence bulk viscous stresses are neglected. The fields $\overline{\rho}$ and $\overline{p}$ denote the coarse-grained density and pressure, whereas $\tilde{\boldsymbol{v}} = \overline{\rho\boldsymbol{v}}/\overline{\rho}$ is the density-weighted coarse-grained velocity as proposed by Reynolds (1895), nowadays called the Favre averaged velocity (Bilger 1975). For a Newtonian fluid, then, the viscous stress tensor reads

$$\tilde{\boldsymbol{\tau}}_{visc} = \eta\left(\boldsymbol{J}_{\tilde{\boldsymbol{v}}} + \boldsymbol{J}_{\tilde{\boldsymbol{v}}}^{\mathrm{T}} - \tfrac{2}{3}\boldsymbol{\nabla}_{\boldsymbol{x}} \cdot \tilde{\boldsymbol{v}}\right), \tag{3.6}$$

with $\boldsymbol{J}_{\tilde{\boldsymbol{v}}}$ the Jacobian of $\tilde{\boldsymbol{v}}$ and $\boldsymbol{J}_{\tilde{\boldsymbol{v}}}^{\mathrm{T}}$ its transpose. The dynamic viscosity η, the reference density $\overline{\rho}_{ref}$ and pressure $\overline{p}_{ref}$, and the speed of sound c_s are dealt with as constant parameters to be specified.

The most important object emerging from the spatial coarse-graining at the arbitrary scale D_K is the SFS tensor $\boldsymbol{\tau}_{SFS}$. It can be formally defined as (Vreman, Geurts & Kuerten 1994; Okraschevski *et al.* 2021*b*)

$$\boldsymbol{\tau}_{SFS}(\boldsymbol{x}, t) := -\int_{V_{\boldsymbol{x}}} \rho(\boldsymbol{y}, t)\,\boldsymbol{w}(\boldsymbol{x}, \boldsymbol{y}, t)\,\boldsymbol{w}^{\mathrm{T}}(\boldsymbol{x}, \boldsymbol{y}, t)\,W(\boldsymbol{x} - \boldsymbol{y})\,\mathrm{d}\boldsymbol{y} = -\overline{\rho\boldsymbol{w}\boldsymbol{w}^{\mathrm{T}}}(\boldsymbol{x}, t), \tag{3.7}$$

with $\boldsymbol{w}$ denoting the peculiar velocity. The peculiar velocity is a relative velocity connecting coarse-grained velocities $\tilde{\boldsymbol{v}}(\boldsymbol{x}, t)$ with associated continuum fluid element velocities $\boldsymbol{v}(\boldsymbol{y}, t)$ (figure 3). By convention, we label and distinguish the spatial coordinates of fluid elements by $\boldsymbol{y} \in \mathbb{R}^3$, and of coarse-grained elements by the spatial coordinate $\boldsymbol{x} \in \mathbb{R}^3$. Consequently, the peculiar velocity is a non-local quantity by definition, and emerges from

$$\boldsymbol{w}(\boldsymbol{x}, \boldsymbol{y}, t) = \boldsymbol{v}(\boldsymbol{y}, t) - \tilde{\boldsymbol{v}}(\boldsymbol{x}, t). \tag{3.8}$$

The velocity decomposition is illustrated in figure 3. We argue that $\boldsymbol{w}$ is the physically appropriate fluctuating velocity field in the coarse-graining framework. It satisfies $\overline{\rho\boldsymbol{w}} = 0$ by construction (Okraschevski *et al.* 2021*b*), and does not require the introduction of generalised central moments to identify the averaging invariance of the turbulent equations (Germano 1992). Since the velocities $\boldsymbol{v}(\boldsymbol{y}, t)$ of the fluid elements are unknown at the coarse-grained level, we practically face the well-known closure problem for the SFS tensor $\boldsymbol{\tau}_{SFS}$ in (3.7).

For turbulent flows at finite resolution, the closure problem is often resolved by explicit modelling of $\boldsymbol{\tau}_{SFS}$ with functional eddy viscosity approaches (Silvis, Remmerswaal & Verstappen 2017; Moser, Haering & Yalla 2021) assuming dominant physical SFS error over discretisation error. However, as long as the filter width and resolution width are

similar, it is well known in the grid-based LES community that these errors are at least of the same order of magnitude, or in fact that the latter exceeds the former (Ghosal 1996; Dairay *et al.* 2017). This insight motivated the development of the nowadays well-established implicit LES approaches, in which the discretisation error is designed to provide the SFS contribution; e.g. Grinstein *et al.* (2007), Moura *et al.* (2017), Dairay *et al.* (2017), Fehn *et al.* (2022), Volpiani (2024). In this light, it is natural to ask how the explicit and implicit SFS contributions in current SPH methods interact. Is it possible to reduce the significant implicit SFS in current SPH methods, emerging from statistical physics principles (Posch *et al.* 1995; Ellero *et al.* 2010; Borreguero *et al.* 2019; Okraschevski *et al.* 2021*a*), using explicit models for τ_{SFS}? This is the leading theme of this work, and in the spirit of similar works in the grid-based LES community (Ghosal 1996; Dairay *et al.* 2017).

4. Methods

There is a large variety of SPH methods today, as contrasted by Eirís *et al.* (2023). Hence care must be taken in the choice of the SPH method for the verification of our incompatibility hypothesis concerning SPH-LES with eddy viscosity models. We decided to use the locally conservative and second-order accurate meshless finite-mass method (MFM), developed and made publicly available in the open source code GIZMO by Hopkins (2015). Since the MFM belongs to the large class of current SPH methods termed MLS-SPH-ALE (Eirís *et al.* 2023), it inherently incorporates both strategies mentioned in § 1 to eliminate the convergence issues of classical SPH. The MFM is based on an ALE formulation without particle shifting, which can be operated in either fully Eulerian or quasi-Lagrangian mode, although we will focus on the latter. (In Appendix A, we perform tests on a Cartesian grid in Eulerian mode to investigate whether the incompatibility is generally related to the SPH method or also influenced by the chosen reference frame. Eventually, we realised that by removing the Lagrangian noise and the induced implicit SFS (figure 1), numerical stability becomes an issue hindering the drawing of a final conclusion. Yet we hypothesise that classical eddy viscosity models will withdraw turbulent kinetic energy mostly from scales larger than the kernel even in an Eulerian frame. This would be the natural consequence of the non-locality that we criticise.) We are convinced that the Lagrangian character is still a key argument for the discretisation of fluid flows with current SPH methods, giving natural access to Lagrangian flow properties such as Lagrangian coherent structures (Haller 2015; Dauch *et al.* 2018). Applying the MFM method to (3.3), (3.4) and (3.5) with a second-order-accurate MLS approximation of spatial derivatives, one arrives, for $i \in \{1, \ldots, N\}$ particles with mass M_i, at

$$\frac{\mathrm{d}M_i}{\mathrm{d}t} = 0 \implies \overline{\rho}_i = M_i \sum_{j=1}^{N_{ngb}} W(\boldsymbol{x}_i - \boldsymbol{x}_j), \tag{4.1}$$

$$M_i \frac{\mathrm{d}\tilde{\boldsymbol{v}}_i}{\mathrm{d}t} = \sum_{j=1}^{N_{ngb}} -\overline{p}_{ij}^* A_{ij}^{eff} + \left[\tilde{\boldsymbol{\tau}}_{visc,ij}^* + \boldsymbol{\tau}_{SFS,ij}^* \right] A_{ij}^{eff}, \tag{4.2}$$

$$\overline{p}_i = \overline{p}_{ref} + c_s^2(\overline{\rho}_i - \overline{\rho}_{ref}), \tag{4.3}$$

where we use standard particle notation. Thus the single index i indicates the numerical proxy of the corresponding field at $\boldsymbol{x}_i$. The discretised momentum equation (4.2) can be interpreted as a Lagrangian finite-volume formulation with fluxes to be approximated at effective interface areas $A_{ij}^{eff} \in \mathbb{R}^3$ between particles i and j. These interface areas depend on the local particle configuration and the chosen kernel, subsequently the pairing-stable

Wendland C4 with $N_{ngb} = 128$ as our default (Dehnen & Aly 2012). The interface fluxes, namely $\overline{p}^*_{ij} \in \mathbb{R}$ and $\tilde{\boldsymbol{\tau}}^*_{visc,ij}, \boldsymbol{\tau}^*_{SFS,ij} \in \mathbb{R}^{3\times3}$, are computed with approximate Riemann solvers that are slope- and flux-limited, and embedded into an explicit single-stage second-order-accurate time integration scheme. More details on the computation of the effective interface areas A^{eff}_{ij}, the Harten–Lax–van Leer contact solver for $\overline{p}^*_{ij}$, the Harten–Lax–van Leer solver for $\tilde{\boldsymbol{\tau}}^*_{visc,ij}, \boldsymbol{\tau}^*_{SFS,ij}$, and aspects beyond that can be found in the works of Hopkins (2015, 2016). We note that the resulting system (4.1), (4.2) and (4.3) is very similar to the well-known classical weakly compressible SPH (WCSPH). Thus we will term it accordingly as weakly compressible MFM (WCMFM). As a consequence of the explicit weakly compressible approach, we expect more Lagrangian noise with stronger implicit SFS due to the allowed acoustic waves, comparing with a stable projection-based incompressible approach at the same resolution (Xu *et al.* 2009; Lind *et al.* 2012). This expectation is not SPH agnostic but seems to be a generally anticipated effect, as demonstrated by Vittoz *et al.* (2019) in a grid-based high-order finite-volume context. After all, the resulting WCMFM discretisation is obviously non-local, realising that the differential operators in the momentum balance of (3.4) are transferred to N_{ngb} flux evaluations per particle on the kernel scale D_K. This is in the spirit of classical SPH (Du & Tian 2020; Vignjevic *et al.* 2021; Yao *et al.* 2022). As will be demonstrated in § 5, it seems to be exactly this non-locality that leads to the incompatibility of SPH-LES with eddy viscosity models for incompressible turbulence (figure 1).

As a canonical benchmark we will consider a Taylor–Green flow (Taylor & Green 1937) on the periodic domain $\Omega = [0, 2\pi]^3$ for three different particle counts $N \in \{128^3, 256^3, 512^3\}$. This is a precious test to evaluate the dissipation characteristics of a numerical solver and its ability to resolve incompressible turbulence; e.g. (Brachet *et al.* 1983; Drikakis *et al.* 2007; Dairay *et al.* 2017; Moura *et al.* 2017; Pereira *et al.* 2021; Fehn *et al.* 2022). As in our former work with classical SPH (Okraschevski *et al.* 2022), we will use the direct numerical simulation (DNS) solution of Dairay *et al.* (2017) at $Re = 10^4$ as a reference. It was computed with the sixth-order finite difference code Incompact3d (Laizet & Li 2011). We will initialise and evaluate the WCMFM simulations exactly as we did in Okraschevski *et al.* (2022) for classical WCSPH. Thus we will specify the initial root mean square Mach number as $Ma_{rms}(t = 0\,\mathrm{s}) = \sqrt{2e_v(t = 0\,\mathrm{s})}/c_s = 0.1$ such that $c_s = 5\,\mathrm{m\,s^{-1}}$, $\overline{\rho}_{ref} = 1\,\mathrm{kg\,m^{-3}}$ and $\overline{p}_{ref} = \overline{\rho}_{ref} c_s^2/4 = 6.25\,\mathrm{Pa}$ in (4.3). Consequently, the dynamic viscosity in (3.6) must be $\eta = 0.0001\,\mathrm{Pa\,s}$ to reach the targeted Reynolds number. We will study and compare the temporal evolution of the averaged kinetic energy e_v, its corresponding averaged dissipation rate $\epsilon_t = -(\mathrm{d}e_v/\mathrm{d}t)$, and the spectral energy density $E(k)$ at $t = 14\,\mathrm{s}$. The time instance was selected in accordance with Dairay *et al.* (2017), which ensures that the turbulence is developed and exhibits the expected inertial range scaling $E(k) \sim k^{-5/3}$ (Kolmogorov 1941; Obukhov 1941; Onsager 1945; Heisenberg 1948). (Note that there is recent experimental doubt about the quantitative correctness of this scaling in the inertial range; see Küchler *et al.* (2023).) For the evaluation of the spectra, we use the validated methodology of Bauer & Springel (2012) in combination with considerations by Durran, Weyn & Menchaca (2017). This preserves physically important small-scale features of the flow, and guarantees the validity of the discrete Parseval relation.

Finally, to work out the interplay between explicit and implicit SFS, we need to specify an explicit SFS model and think about how the implicit SFS contribution can be estimated. For the former, we decided to opt for the σ model by Nicoud *et al.* (2011), which is one of the most sophisticated static eddy viscosity models. It eliminates artificial dissipation in two-dimensional flows, laminar shear zones and solid body rotation, but likewise shows

proper asymptotic scaling near walls (Nicoud *et al.* 2011; Silvis *et al.* 2017; Moser *et al.* 2021). The explicit model reads in continuous representation

$$\boldsymbol{\tau}_{SFS}^{exp} = \eta_{SFS} \left(\boldsymbol{J}_{\tilde{\boldsymbol{v}}} + \boldsymbol{J}_{\tilde{\boldsymbol{v}}}^{\mathrm{T}} - \frac{2}{3} \boldsymbol{\nabla}_x \cdot \tilde{\boldsymbol{v}} \right), \quad \eta_{SFS} := \overline{\rho}(C_\sigma \varDelta)^2 \frac{(\sigma_1 - \sigma_2)(\sigma_2 - \sigma_3)\sigma_3}{\sigma_1^2}, \quad (4.4)$$

where σ_k, $k \in \{1, 2, 3\}$, are the singular values of the tensor $\boldsymbol{J}_{\tilde{\boldsymbol{v}}}^{\mathrm{T}} \boldsymbol{J}_{\tilde{\boldsymbol{v}}}$, $C_\sigma = 1.35$ is a model constant, and the filter width is $\varDelta = D_K$. The latter is an unambiguous choice emerging from our coarse-graining perspective and a matter of debate in the SPH-LES context (Rennehan 2021; King *et al.* 2023). We will elaborate on it more closely in § 5. For the estimation of the implicit SFS tensor, we assume that density changes of the fluid elements over the kernel scale D_K are much weaker than the corresponding velocity changes. This is reasonable for a weakly compressible flow developing characteristics of incompressible turbulence, and implies that $\tilde{\boldsymbol{v}} = \overline{\boldsymbol{v}}$. Then with the spatial coarse-graining operation in (3.2) and linearisation of the continuum velocity field at a position $\boldsymbol{z} \in \mathbb{R}^3$, one obtains $\tilde{\boldsymbol{v}}(\boldsymbol{x} = \boldsymbol{z}, t) = \boldsymbol{v}(\boldsymbol{y} = \boldsymbol{z}, t) + O(D_K^2)$, which gives a consistency preserving (with respect to the MFM discretisation) second-order proxy for the peculiar velocity in (3.8), namely

$$\boldsymbol{w}(\boldsymbol{x}_1, \boldsymbol{x}_2, t) \approx \tilde{\boldsymbol{v}}(\boldsymbol{x}_2, t) - \tilde{\boldsymbol{v}}(\boldsymbol{x}_1, t), \quad (4.5)$$

with two different coarse-grained coordinates $\boldsymbol{x}_1$, $\boldsymbol{x}_2$. Inserting (4.5) into the SFS tensor in (3.7) gives, after discretisation of the integral into finite-mass elements, the following estimator for the implicit SFS in particle notation:

$$\boldsymbol{\tau}_{SFS,i}^{imp} \approx - \sum_{j=1}^{N_{ngb}} (\tilde{\boldsymbol{v}}_j - \tilde{\boldsymbol{v}}_i)(\tilde{\boldsymbol{v}}_j - \tilde{\boldsymbol{v}}_i)^{\mathrm{T}} W(\boldsymbol{x}_i - \boldsymbol{x}_j) M_j. \quad (4.6)$$

Since incompressible turbulence is a convection-driven phenomenon, we will evaluate the local importance of the implicit SFS on a particle i in comparison to the coarse-grained convective stress tensor $\overline{\rho}_i \tilde{\boldsymbol{v}}_i \tilde{\boldsymbol{v}}_i^{\mathrm{T}}$. Therefore, we define the R-index as

$$R_i := \frac{\|\boldsymbol{\tau}_{SFS,i}^{imp}\|_F}{\|\boldsymbol{\tau}_{SFS,i}^{imp}\|_F + \|\overline{\rho}_i \tilde{\boldsymbol{v}}_i \tilde{\boldsymbol{v}}_i^{\mathrm{T}}\|_F}, \quad (4.7)$$

with $\| \cdot \|_F$ denoting the Frobenius norm.

5. Results and discussion

In this section, we will present and critically discuss the results of our study. We start with a qualitative verification of our implementation of the σ model (Nicoud *et al.* 2011) in (4.4) into the code GIZMO (Hopkins 2015). Therefore, the uniquely coloured individual particle IDs are utilised as flow tracers and visualised for the purpose of structure identification (figure 4). Two snapshots before and after the well-known dissipation peak (Brachet *et al.* 1983), namely at $t_{1,2} = 9 \pm 3$ s, are shown in figures 4(*a,c*) and 4(*b,d*), respectively, for the highest resolution runs $N = 512^3$. They vividly render the development of primary instabilities and turbulence in the flow field. Figure 4(*a,b*) display the case without explicit SFS model (WCMFM), and figure 4(*c,d*) with explicit SFS model (WCMFM + SIGMA). In figure 4(*e,f*), the central quantity of the σ model, namely the eddy viscosity field according to (4.4), is shown. It is scaled by the dynamic viscosity of the flow. The ratio, denoted as η^*, visually correlates with the flow structures and is evidently non-negligible in the shear flow planes (figure 4*a*) where incompressible turbulence develops. In this
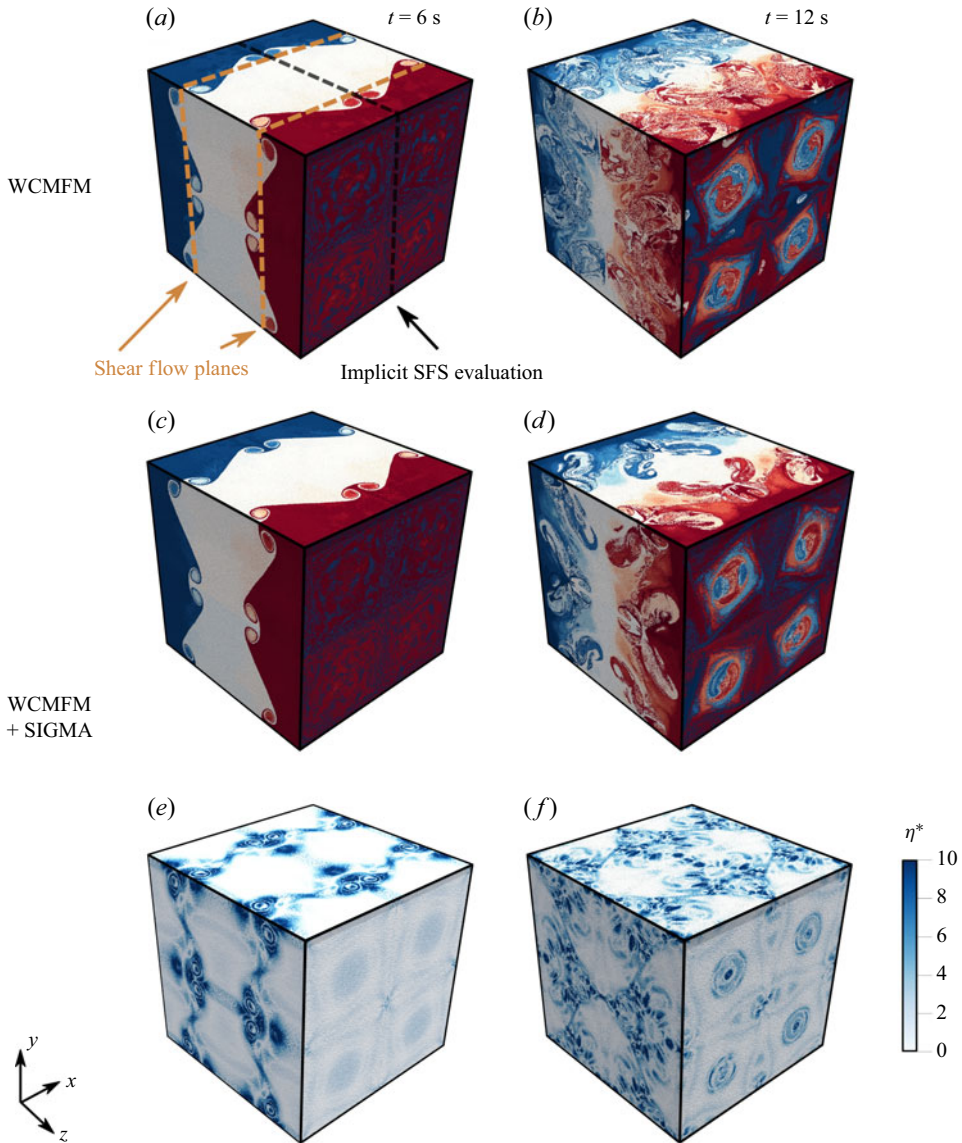
Figure 4. Qualitative verification of the implementation of the σ model (Nicoud *et al.* 2011) for $N = 512^3$. Flow structures before and after the dissipation peak (*a,b*) for the case without explicit SFS model (WCMFM), and (*c,d*) for the case with explicit SFS model (WCMFM + SIGMA). (*e,f*) The scaled eddy viscosity field.

region, the eddy viscosity is dominant over the dynamic viscosity by up to an order of magnitude. This is an anticipated consequence as the coarse-grained viscous stress tensor is bounded from above by the Cauchy–Schwarz inequality, and it can be proven that the bound scales with $1/D_K$ (Eyink & Drivas 2018). Hence for regions of under-resolved turbulence, in which the kernel scale D_K is larger than viscous length scale, one would expect $\eta^* \gg 1$. A comparison of the flow structures predicted by WCMFM and WCMFM + SIGMA reveals that the explicit SFS model does not inhibit the dynamics of the primary instabilities before the dissipation peak (figure 4*a* versus figure 4*c*). However, it apparently damps noisy small-scale features in the turbulent flow field after
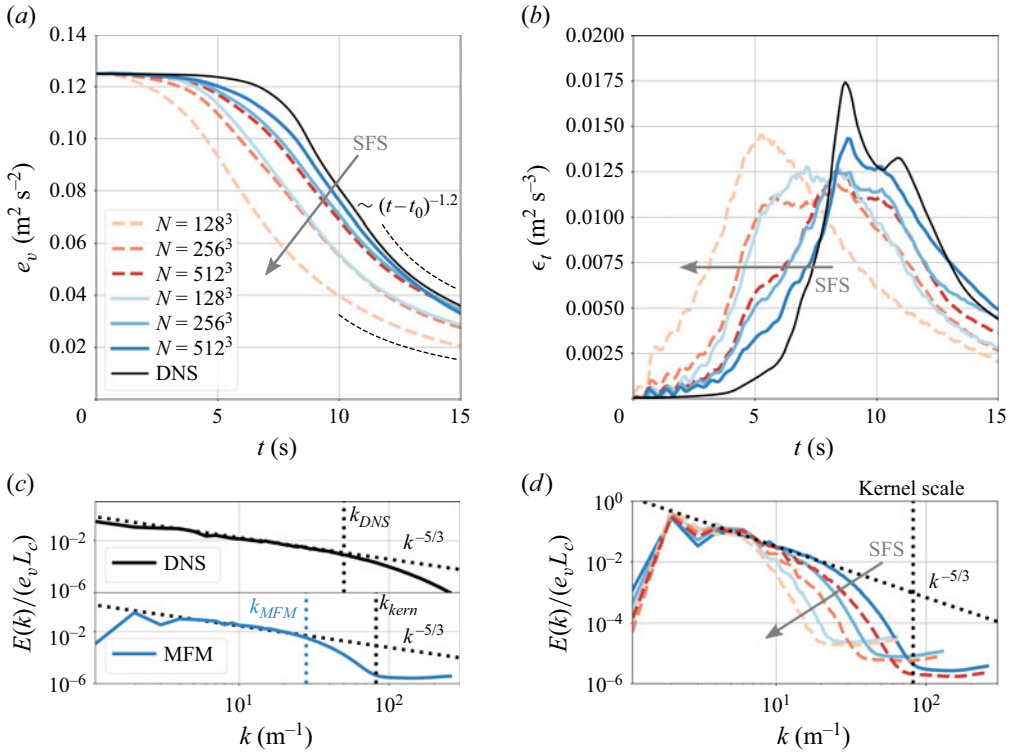
Figure 5. Quantitative effect of the σ model (Nicoud *et al.* 2011) in physical and spectral space for different resolutions: (*a*) averaged kinetic energy; (*b*) averaged dissipation rate; (*c*) scaled spectral energy density at $t = 14$ s for DNS and WCMFM run ($N = 512^3$) without explicit SFS model; (*d*) scaled spectral energy density at $t = 14$ s. For orientation, the kernel scale for $N = 512^3$ is included.

the dissipation peak (figure 4*b* versus figure 4*d*). This could be incorrectly interpreted as removal of numerically dissipative Lagrangian noise (artificial thermalisation). As extensively discussed by Dairay *et al.* (2017) for grid-based methods, the removal of such an artificial thermalisation should be the ultimate goal of an explicit SFS model, eventually resulting in a quantitative improvement for the dissipation characteristics in physical and spectral space. We will show now that the explicit SFS model completely fails with respect to such a quantitative analysis, although visually it seems to perform well.

Therefore, we compare the temporal evolution of the averaged kinetic energy e_v, the averaged dissipation rate ϵ_t and the spectral energy density $E(k, t = 14$ s) in figure 5. The latter is scaled with the corresponding kinetic energy value $e_v(t = 14$ s) and $L_c = 1$ m, such that integration over the wavenumber shells always results in unity. Cases without explicit SFS model (WCMFM) are displayed as solid blue lines, whereas cases with explicit SFS model (WCMFM + SIGMA) are displayed as red dashed lines. It is evident for the kinetic energy evolution in figure 5(*a*) that qualitative convergence towards the DNS (solid black line) for increasing particle count can be obtained. After the dissipation peak, as soon as incompressible turbulence develops, the theoretically predicted Saffman decay rate (Skrbek & Stalp 2000) $e_v \sim (t - t_0)^{-1.2}$ can be matched (dashed black line). Here, t_0 denotes a time shift parameter that accounts for the earlier transitions at lower resolution. These observations are independent of the explicit SFS model and also reflected by the dissipation rate profiles in figure 5(*b*). However, the results clearly demonstrate

the detrimental effect of the eddy viscosity model on the dissipation characteristics in physical space. Coincidentally, for the chosen configuration, it seems that the explicit SFS model leads to a fallback of the accuracy by approximately a whole resolution step. The WCMFM cases for $N = 128^3$ and $N = 256^3$ behave very similar to the WCMFM + SIGMA cases for $N = 256^3$ and $N = 512^3$. In other words, under ideal code scaling with CFL restriction, to achieve the same result with an explicit SFS model, at least a $2^4 = 16$ times higher computational effort is required. This is a quite drastic finding. Note that for a quasi-Lagrangian particle method, the highest-resolution WCMFM run ($N = 512^3$) without explicit SFS model leads to a comparably accurate prediction of the dissipation characteristics in physical space. In particular, the sharper prediction of the global dissipation peak and the local peak nearby in figure 5(*b*) compared to WCSPH with twice as many neighbours (Okraschevski *et al.* 2022) is prominent.

Before we proceed with the comparison on the spectral dissipation characteristics for all resolutions, we will first elaborate on the highest-resolution WCMFM run in figure 5(*c*). Provably, WCMFM as current SPH method is able to predict the inertial range scaling of incompressible turbulence by approximately an order of magnitude in wavenumber space. However, in comparison to the DNS case, the inertial range already terminates at $k_{MFM} < k_{DNS}$ (by k_{MFM} we denote the effective wavenumber up to which a qualitatively correct spectral behaviour can be observed and not the wavenumber corresponding to the mean particle diameter Δl), then passes into the energy deficit range $k \in [k_{MFM}, k_{kern}]$ and is followed by the Lagrangian noise range (artificial thermalisation) resulting from kernel scale errors. Qualitatively, this is similar to classical SPH, and happens although the kernel wavelength satisfies $k_{kern} > k_{DNS}$ (Okraschevski *et al.* 2022). It is indicative for the non-local character of the method, the emerging implicit SFS according to (4.6) and a reaction to peculiar velocities on the kernel scale, which manifest as artificial thermalisation. In the next paragraph this will be detailed, but prior to that we want to show in figure 5(*d*) that the explicit SFS model also deteriorates the situation in spectral space due to the non-locality of the method. Instead of removing a significant part of kinetic energy from the artificial thermalisation, it dominantly withdraws kinetic energy from the energy deficit range and the partially resolved inertial range. Hence it erroneously attacks scales that are already badly resolved, and not the numerically dissipative ones. While these observations should be sufficient to advise against the usage of classical eddy viscosity models in the SPH-LES context, we want to unravel the interplay of the implicit SFS and explicit SFS models in the following paragraph, and underpin these spectral observations in physical space.

Ergo, we will visualise the implicit SFS relative to the convective stress using the R-index defined in (4.7), and investigate how the field is affected by resolution and the explicit SFS model. We will focus on the plane $x = \pi$ (figure 4*a*) for the time $t = 14$ s, exactly corresponding to the spectra in figures 5(*c*) and 5(*d*). The resulting fields are depicted in figure 6 and contain a kernel element at the given resolution in the upper right corner to assess the extent of emerging coherent structures. We will start with the influence of the spatial resolution for WCMFM without explicit SFS model shown in figure 6(*a,c,e*). Note that due to the definition of the R-index, the exact ratio of implicit SFS to the convective stress is given by $\|\boldsymbol{\tau}_{SFS,i}^{imp}\|_F / \|\overline{\rho}_i \tilde{\boldsymbol{v}}_i \tilde{\boldsymbol{v}}_i^{\mathrm{T}}\|_F = R_i/(1 - R_i)$, and the upper limit of the colour bar indicates that the implicit SFS is a third of the convective stress. Interestingly, for all resolutions, the implicit SFS is relevant only around the shear flow planes where incompressible turbulence develops and forms a coherent network that surpasses the kernel scale; although the coherent network becomes more delicate for higher resolution (cf. figure 6*a,e*), structures with significant contribution remain larger in extent than the given kernel element. Considering that the implicit SFS is a consequence
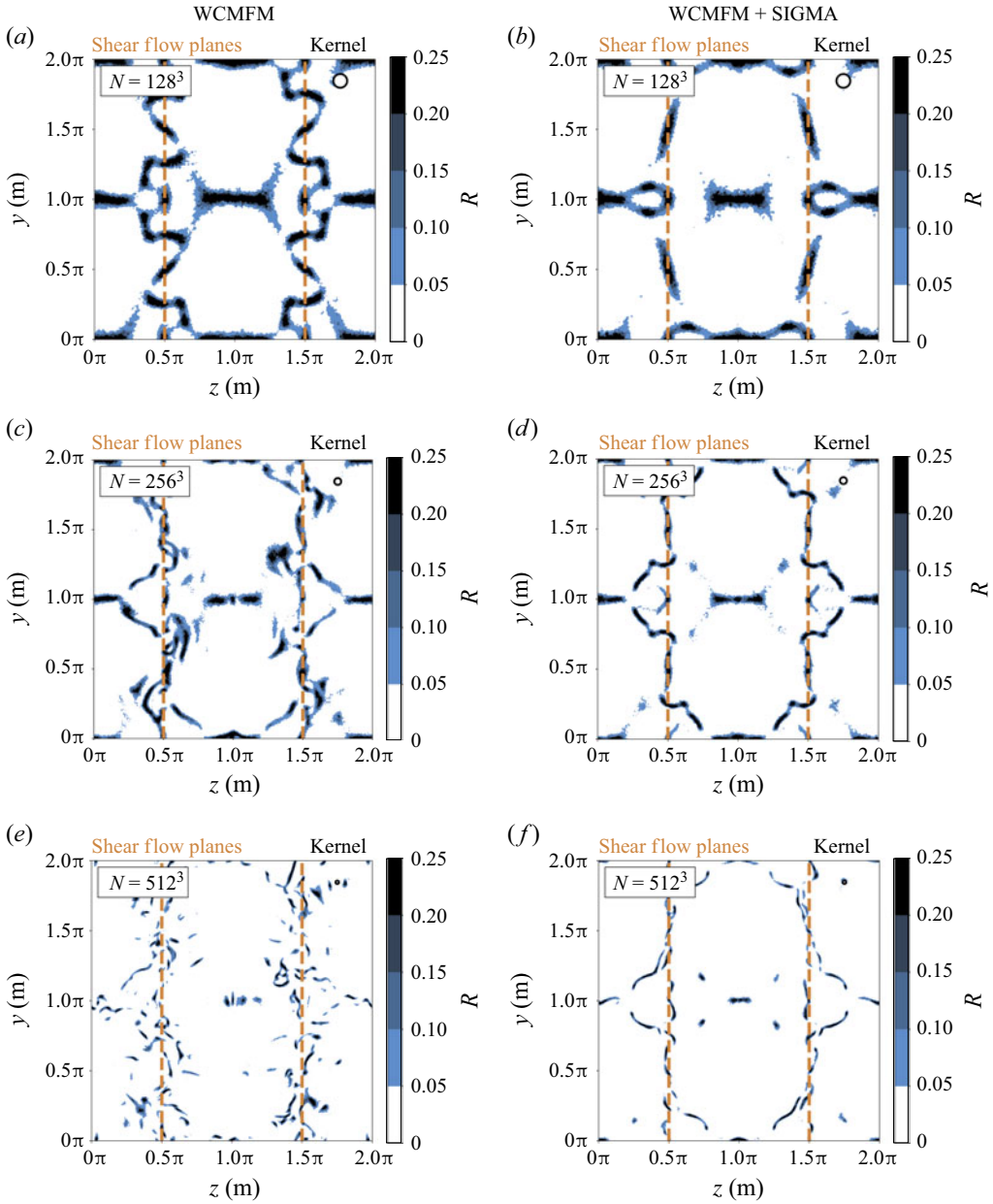
Figure 6. Implicit SFS measured by the R-index in (4.7) at the plane $x = \pi$ for the time $t = 14$ s. Different resolutions are shown without explicit SFS model (WCMFM) and with explicit SFS model (WCMFM + SIGMA).

of the peculiar velocities evaluated at the kernel scale but unfolds its effect well beyond the kernel scale, we believe we can see the deterministic reason for how the artificial thermalisation causes the energy deficit range in spectral space (figure 5c,d). Hence the $\|\boldsymbol{\tau}_{SFS,i}^{imp}\|_F$ field unravels how the kernel scale effects propagate to larger scales due to the non-local character of the method. Focusing now on figure 6(b,d,f), in which the WCMFM + SIGMA cases are shown, a reflection of the spectral behaviour in figure 5(d)

can be clearly seen as well. Even though we would expect a working explicit SFS model to significantly reduce $\|\boldsymbol{\tau}_{SFS,i}^{imp}\|_F$ with respect to R on the kernel scale, we see a strong non-local damping. The network itself is destroyed, instead of diminishing its amplitude. Recalling the similarity of the WCMFM cases for $N = 128^3$ and $N = 256^3$, and WCMFM + SIGMA cases for $N = 256^3$ and $N = 512^3$ in physical space highlighted above, our requirements on a working explicit SFS model can be specified more precisely. It manifests in the comparison of figures 6(*a*) versus 6(*d*), and figures 6(*c*) versus 6(*f*). There, the network structure is mainly preserved, and the amplitude of R diminished. Together with the spectral statistics in figure 5(*d*), it is evident that this observation correlates with a diminished artificial thermalisation and gain in the energy deficit range. This is what we would expect from an explicit SFS model in the SPH-LES context in a much stronger form for a fixed resolution, but unfortunately see that even sophisticated eddy viscosity models, such as the σ model by Nicoud *et al.* (2011), fail.

Taking this new evidence for a current SPH method into account with our former, congruent results for classical SPH (Okraschevski *et al.* 2022), we are convinced that SPH-LES with classical eddy viscosity models is highly detrimental for the prediction of incompressible turbulence. In our opinion, this is due to the mismatch of discretisation characteristics, namely quasi-Lagrangian particles and non-locality, with the explicit SFS model therefore being spectrally introduced in the already problematic energy deficit range. We observe the well-known issue from grid-based LES that an *a priori* correct model can perform badly in simulations *a posteriori* (Park, Yoo & Choi 2004; Dairay *et al.* 2017). From our coarse-graining perspective, current SPH methods operate intrinsically as Lagrangian LES with implicit SFS for incompressible turbulence. We want to stress that the chosen terminology is not indicative of the quality of this implicit LES approach, which manifests in the spectral energy density in figure 5(*c*). Obviously, it is plagued by an energy deficit range due to artificial thermalisation. We have shown already in our former work that the inertial range can be reproduced with grid-based finite-volume Smagorinsky LES at much lower resolution $N = 384^3$ and lower computational cost (Okraschevski *et al.* 2022).

Before we finally conclude our work, we want to address two more aspects that are no less important: first, the effect of the filter width Δ when using an explicit SFS model; and second, the effect of the neighbour particles N_{ngb} for simulations without explicit SFS model. The results are displayed in figure 7 for all cases considering $N = 256^3$.

The first aspect is an ongoing matter of debate in the SPH-LES context (Rennehan 2021; King *et al.* 2023). Although from our coarse-graining perspective the choice $\Delta = D_K$ is unambiguous, we have considered the two further cases with $\Delta = D_K/2$ (Rennehan 2021) and $\Delta = 2D_K$. The case $\Delta = 0$ corresponds to the run without an explicit SFS model. Obviously from figures 7(*a*) and 7(*c*), we observe a monotonic trend with increasing filter width. The effect is detrimental in physical space as well as in spectral space, but starts to get irrelevant for $\Delta \leqslant D_K/2$. This is congruent with the observation of Rennehan (2021), who studied forced subsonic turbulence with MFM and different explicit SFS models using a dynamic procedure. It prompts the eventuality that SPH-LES studies with Δ equal to or smaller than the kernel radius – e.g. Antuono *et al.* (2021*b*), Colagrossi *et al.* (2021), Lai *et al.* (2022), King *et al.* (2023) – just run (slightly) more expensive simulations in which the influence of the explicit SFS model is negligible.

The second aspect concerns the influence of the number of neighbours N_{ngb} for WCMFM without explicit SFS model. In classical SPH, better convergence towards the DNS can be obtained by increasing N_{ngb} (Zhu *et al.* 2015; Okraschevski *et al.* 2022), which is in the spirit of explicitly filtered LES (Lund 2003; Bose, Moin & You 2010).
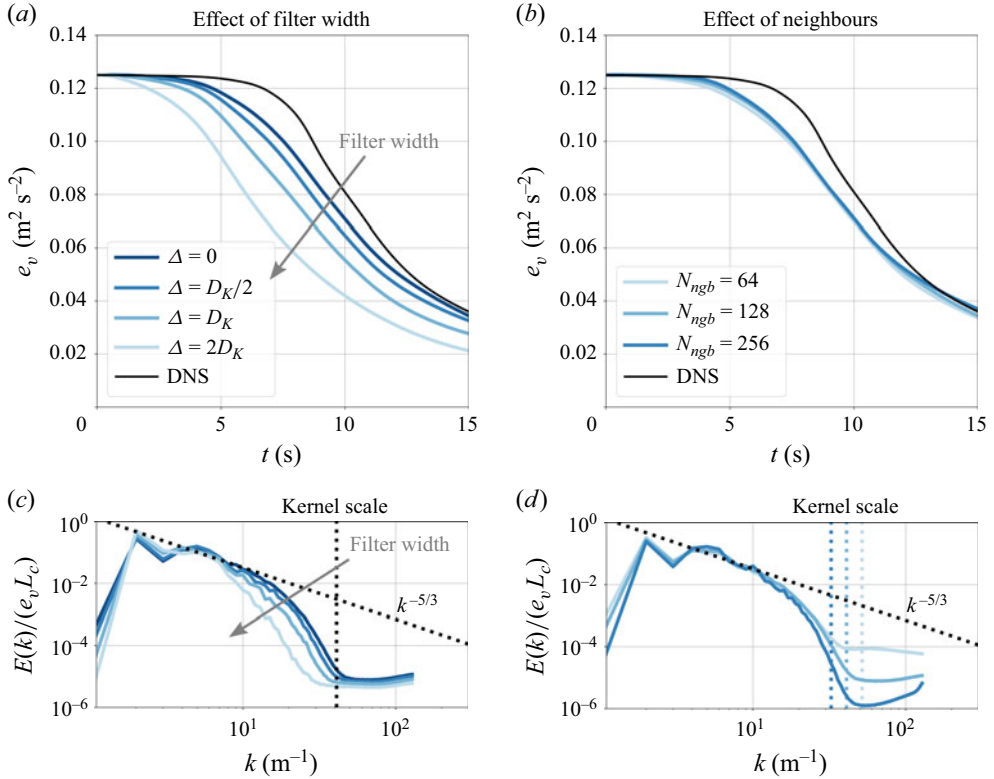
Figure 7. (*a,c*) Influence of the filter width Δ for WCMFM + SIGMA, and (*b,d*) the neighbour particles N_{ngb} for WCMFM without explicit SFS model. All simulations were performed with $N = 256^3$.

However, for current SPH methods as MFM one would expect minor influence of N_{ngb} by construction (Vila 1999; Hopkins 2015). Indeed, a negligible influence is found according to figures 7(*b*) and 7(*d*) for the well-resolved scales. Merely in spectral space, we see a loss of kinetic energy from the artificial thermalisation and the energy deficit range that seems irrelevant for the physical space dynamics. This is contrary to classical SPH, practically eliminates N_{ngb} as a crucial calibration parameter, and is beneficial for the computational cost at finite resolution. Coincidentally, we observe for $N_{ngb} \neq 128$ that the associated kernel scale in figure 7(*d*) is not perfectly separating the energy deficit range and the artificial thermalisation as in the former cases.

6. Concluding remarks

In this study, we presented evidence for the incompatibility of current SPH methods and classical eddy viscosity models for scale-resolved incompressible turbulence. This result is of particular importance for current SPH methods, which are often advantageously applied in complex multiphase flows potentially encompassing incompressible turbulence (Colagrossi *et al.* 2021; Lai *et al.* 2022; King *et al.* 2023; Meringolo *et al.* 2023). With our coarse-graining perspective, we could argue and show for MFM, as a representative from the class of MLS-SPH-ALE approaches (Eirís *et al.* 2023), that it intrinsically operates as Lagrangian LES with significant implicit SFS. Even a sophisticated eddy viscosity model such as the σ model by Nicoud *et al.* (2011) is not able to reduce this implicit SFS due to the non-locality of the discretisation method. For the unambiguous filter width $\Delta = D_k$,

the explicit SFS model attacks dominant scales larger than the kernel that are already underresolved. Hence the explicit SFS model is either highly detrimental physically, or for choices $\Delta \leqslant D_K/2$, is likely irrelevant and introduces computational overhead. The latter complies with results of Rennehan (2021). To our knowledge, such a study of the interplay between implicit SFS and explicit SFS models for a current SPH method is presented for the first time, revealing the familiar *a priori* versus *a posteriori* dilemma in grid-based LES; e.g. Park *et al.* (2004), Dairay *et al.* (2017). It elucidates that SPH-LES approaches, even with current SPH methods, must focus on the mitigation of the implicit SFS to improve the predictive power of the Lagrangian LES. In particular, one core application area of SPH, namely multiphase flows, could benefit from it if turbulence matters. This progress can be realised either directly by completely new explicit SFS models, which match the discretisation characteristics of current SPH methods, or indirectly by numerical noise mitigation techniques.

Hypothetically, in this work there exist two disregarded mainstream aspects of current SPH methods compliant with the latter strategy. Particle shifting (Xu *et al.* 2009; Lind *et al.* 2012) and density diffusion (Antuono *et al.* 2010; Marrone *et al.* 2011) are established numerical noise mitigation techniques, also in the SPH-LES context (Antuono *et al.* 2021*a*,*b*; Colagrossi *et al.* 2021; Meringolo *et al.* 2023). It is likely that both reduce the peculiar velocities on the kernel scale according to (4.5), and indirectly have positive feedback on the implicit SFS according to (4.6). However, we believe that the density diffusion, which can be heuristically rationalised by a coarse-graining without the density-weighted Favre velocity (Di Mascio *et al.* 2017), will also be plagued by non-local effects of the discretisation scheme. Very likely, it will mitigate not only noisy but also physically under-resolved scales. Nevertheless, this needs to be tested in follow-up studies.

Another concluding point that needs to be stressed is that our coarse-graining theory is valid only for $D_K \approx$ const. and $\rho \approx$ const., hence when compressibility effects are negligible. This is what we ensured by our initial root mean square Mach number choice $Ma_{rms}(t = 0\,\text{s}) = \sqrt{2e_v(t = 0\,\text{s})}/c_s = 0.1 < 0.3$ (Jakobsen 2014) for the decaying Taylor–Green flow at $Re = 10^4$. Considering this aspect, an essential difference between our results and the results of Rennehan (2021) should be highlighted. The energy deficit range observed in this study and our former one for classical SPH (Okraschevski *et al.* 2022) is there replaced by an energy pile-up known from highly accurate discontinuous Galerkin methods (Moura *et al.* 2017; Fehn *et al.* 2022). We believe that this difference is rooted in the Mach number at which the spectral statistics are computed. Whereas $Ma_{rms} \approx 0.3$ is controlled by forcing in Rennehan (2021), the Mach number in our decaying case can be estimated to be $Ma_{rms}(t = 14\,\text{s}) = \sqrt{2e_v(t = 14\,\text{s})}/c_s \approx 0.06$. It was already shown by Hopkins (2015) that the accuracy of the MFM method deteriorates with lower Mach number, possibly explaining the switch from the energy pile-up to the energy deficit also known from classical SPH. Such low Mach numbers are not unusual in engineering applications, and favourably comply with our coarse-graining theory.

For completeness, we would like to bring up that alternative Lagrangian LES approaches exist that are much better suited to accurately predict incompressible turbulence, if the latter is the exclusive goal. These are the so-called vortex particle methods (Alvarez & Ning 2024), which solve the Navier–Stokes equations in their velocity–vorticity form by a decomposition of the fields into self-adaptive Lagrangian vortex elements. Interestingly, these methods suffer from the exact opposite picture developed in this work for current SPH methods, namely insufficient implicit SFS to obtain stability. In order to restore the latter, explicit SFS models seem inevitable (Mansfield *et al.* 1998, 1999; Alvarez & Ning 2024). This said, one might wonder whether there is a chance to develop a Lagrangian LES method to retain the high accuracy of the vortex particle methods for incompressible

turbulence and flexibility and robustness of current SPH methods required for complex multiphase flows. A promising machine-learning based route towards such an ultimate goal could be the one presented by Woodward *et al.* (2023) and Tian *et al.* (2023).

Appendix A. Incompatibility in the Eulerian reference frame?

In order to elaborate on the influence of the chosen reference frame, we repeated the numerical experiments presented in § 5 in a fully Eulerian mode for $N = 256^3$. The GIZMO code permits such a course of action as it is methodologically based on an MLS-SPH-ALE framework. The underlying idea is to remove the Lagrangian noise (Hopkins 2015; Lind & Stansby 2016) and the corresponding implicit SFS by construction to clearly isolate the effect of the explicit SFS model. This allows us to analyse whether the incompatibility of classical eddy viscosity models with current SPH methods, rooted in the non-local discretisation, persists in an Eulerian reference frame.

The results for the same parameters and initial conditions are shown in figure 8(*a*). Obviously, the numerical dissipation solely introduced by the approximate Riemann solvers for the interface fluxes (§ 4) is not sufficient to obtain a stable solution, even leading to a blow-up of kinetic energy beyond $t > 10$ s in the Eulerian case. Although the σ model by Nicoud *et al.* (2011) can prevent the blow-up (Eulerian + SFS), it seems not appropriate to eradicate the actual cause of the instability as the kinetic energy starts to plateau beyond $t > 10$ s, also developing oscillatory behaviour. The instability is rooted in constructively interfering acoustic waves leading to density changes of 30 % deviation from $\overline{\rho}_{ref} = 1$ kg m^{-3} (not shown herein), which is in contrast to the allowed magnitude of our explicit weakly compressible approach for the targeted $Ma_{rms} \leqslant 0.1$ (§ 4). We will now show that these interfering acoustic waves cannot be eliminated in the Eulerian reference frame with numerical adaptions in GIZMO, unfortunately hindering the drawing of a final conclusion in terms of generalisation of the incompatibility that we observe in the Lagrangian mode. This interference remains even if we switch to the most dissipative numerical scheme in GIZMO (figure 8*f*).

As noted by Hopkins (2015), the slope-limiting procedure specifically designed and calibrated for his MLS-SPH-ALE methods in the Lagrangian reference frame must be likely adapted to more conservative parameters in the context of Cartesian grids in an Eulerian mode. Using the most conservative choice in GIZMO, available as a pre-processor directive (SLOPE_LIMITER_TOLERANCE = 0), results in the averaged kinetic energy evolution in figure 8(*b*). Although this gives a stable result, we obtain seemingly sub-dissipative behaviour in the kinetic energy after $t > 6$ s, and adding the explicit SFS model does not lead to qualitative improvement. However, realising that the Eulerian run without SFS can perfectly match the kinetic energy characteristics up to $t \leqslant 6$ s, we additionally exchanged the Harten–Lax–van Leer contact flux approximation by the central Kurganov–Tadmor scheme (Kurganov & Tadmor 2000; Panuelos, Wadsley & Kevlahan 2020) without the novel dissipation switch developed by Panuelos *et al.* (2020). This should give the most dissipative Eulerian run on a Cartesian grid in GIZMO, and hopefully eliminate the seemingly sub-dissipative behaviour observed
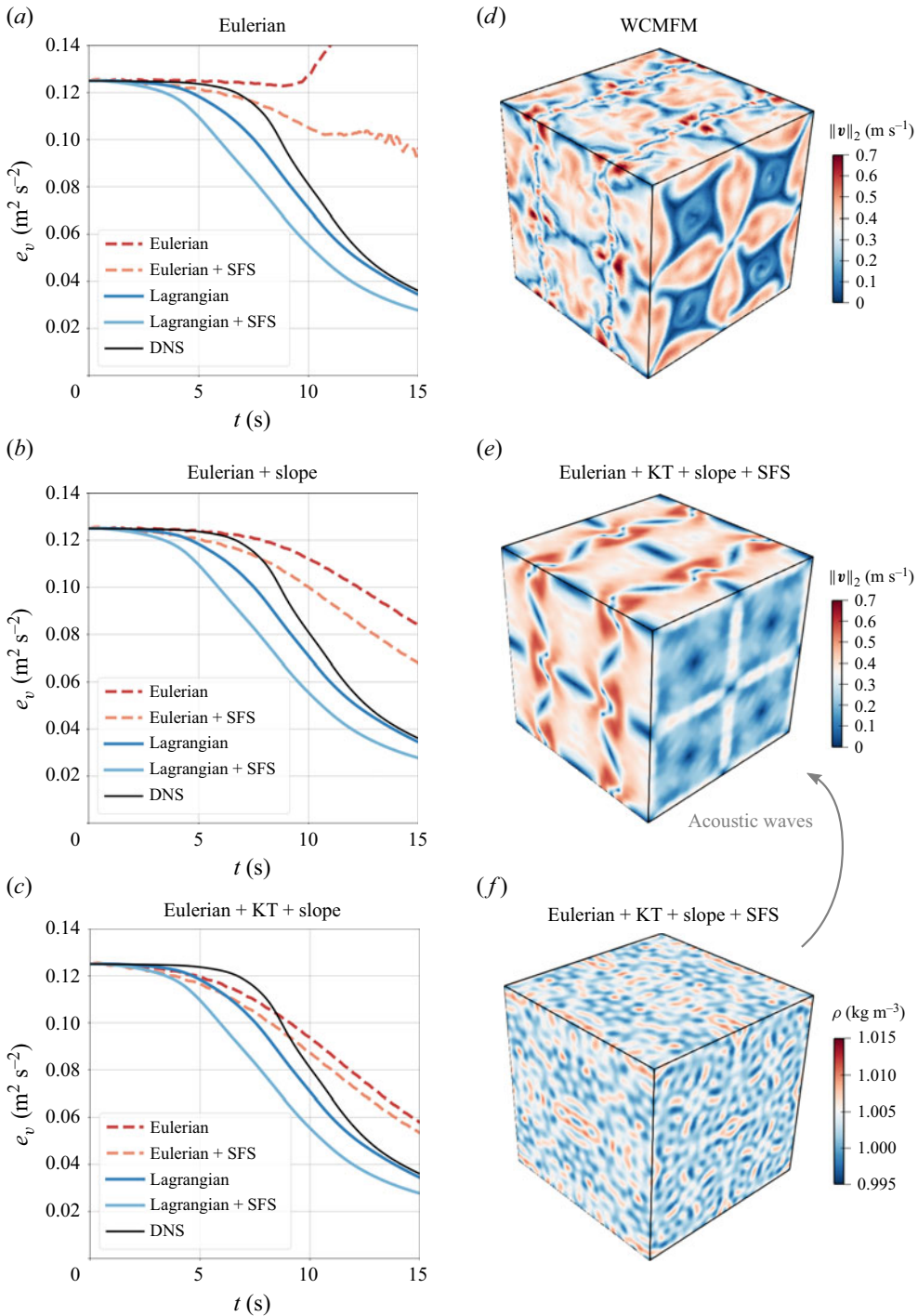
Figure 8. Comparison of Lagrangian and Eulerian results for $N = 256^3$. (a) Averaged kinetic energy with same parameters. (b) Averaged kinetic energy with conservative slope limiter. (c) Averaged kinetic energy with Kurganov–Tadmor (KT) scheme and conservative slope limiter. (d) Velocity magnitude at $t = 14$ s from the Lagrangian WCMFM run without SFS. (e) The Eulerian run with Kurganov–Tadmor scheme and conservative slope limiter and SFS. (f) The corresponding density field of the latter.

before. Evidently from figure 8(*c*), the overall dissipation increases from the beginning, but the sub-dissipative behaviour persists while it is shifted to $t > 9$ s. Again, the explicit SFS model does not qualitatively improve this situation. To rationalise these effects, the magnitude of the velocity fields from the least dissipative Lagrangian run (figure 8*d*) and the most dissipative Eulerian run (figure 8*e*) can be compared at $t = 14$ s, where incompressible turbulence should be present. Apparently, taking all dissipation measures into account, the Eulerian velocity field is much smoother than the Lagrangian reference, even showing a laminarisation of the dynamics in the shear flow planes. This is surprising, given that the averaged kinetic energy levels exceed the Lagrangian ones after $t > 9$ s (figure 8*c*). Actually, a decrease of the (effective) Reynolds number should result in a monotonic decrease in the averaged kinetic energy levels (Fehn *et al.* 2022). Hence kinetic energy must be introduced by another mechanism. These are the constructively interfering acoustic waves mentioned above, which manifest in the corresponding density field in figure 8(*f*). Although their magnitude is reasonable in terms of the weakly compressible approach taking all dissipation measures into account, they are the dominant, unphysical feature in the density field. Unfortunately, they also introduce oscillatory behaviour in the velocity field (figure 8*e*) and are the root of instability in figure 8(*a*) and the seemingly sub-dissipative behaviour in figure 8(*b*,*c*).

From these observations, we extract three main conclusions.

(i) To perform implicit LES of incompressible turbulence with the MLS-SPH-ALE methods of Hopkins (2015), the Lagrangian reference frame with its Lagrangian noise and the related implicit SFS seem inevitable. In the Eulerian frame, the numerical schemes lack a direct dissipation mechanism for the detrimental acoustic waves.

(ii) If an implicit LES in an Eulerian reference frame were possible, then we would expect that the incompatibility of classical eddy viscosity models and current SPH methods persists as it is rooted in the non-local discretisation.

(iii) The σ model by Nicoud *et al.* (2011) does not resolve the acoustic wave issue due to a lack of awareness. This could also be interpreted as a sort of incompatibility, but is different from the non-local incompatibility to which we refer in our work.

REFERENCES

ALVAREZ, E.J. & NING, A. 2024 Stable vortex particle method formulation for meshless large-eddy simulation. *AIAA J.* **62** (2), 637–656.

ANTUONO, M., COLAGROSS, A., MARRONE, S. & MOLTENI, D. 2010 Free-surface flows solved by means of SPH schemes with numerical diffusive terms. *Comput. Phys. Commun.* **181** (3), 532–549.

ANTUONO, M., MARRONE, S., MASCIO, A.DI & COLAGROSSI, A. 2021*a* Smoothed particle hydrodynamics method from a large eddy simulation perspective. Generalization to a quasi-Lagrangian model. *Phys. Fluids* **33**, 015102.

ANTUONO, M., SUN, P.N., MARRONE, S. & COLAGROSSI, A. 2021*b* The δ-ALE-SPH model: an arbitrary Lagrangian–Eulerian framework for the δ-SPH model with particle shifting technique. *Comput. Fluids* **216**, 104806.

BAUER, A. & SPRINGEL, V. 2012 Subsonic turbulence in smoothed particle hydrodynamics and moving-mesh simulations. *Mon. Not. R. Astron. Soc.* **423**, 2558.

BICKNELL, G.V. 1991 The equations of motion of particles in smoothed particle hydrodynamics. *SIAM J. Sci. Stat. Comput.* **12**, 1198–1206.

BILGER, R.W. 1975 A note on Favre averaging in variable density flows. *Combust. Sci. Technol.* **11**, 215–217.

BORREGUERO, M., BEZGIN, D., ADAMI, S. & ADAMS, N.A. 2019 Implicit atomistic viscosities in smoothed dissipative particle dynamics. *Phys. Rev. E* **100**, 033318.

BOSE, S.T., MOIN, P. & YOU, D. 2010 Grid-independent large-eddy simulation using explicit filtering. *Phys. Fluids* **22** (10), 105103.

BRACHET, M., MEIRON, D., ORSZAG, S., NICKEL, B., MORF, R. & FRISCH, U. 1983 Small-scale structure of the Taylor–Green vortex. *J. Fluid Mech.* **130**, 411–452.

COLAGROSSI, A., MARRONE, S., COLAGROSSI, P. & TOUZÉ, D.L. 2021 Da Vinci's observation of turbulence: a French–Italian study aiming at numerically reproducing the physics behind one of his drawings, 500 years later. *Phys. Fluids* **33** (11), 115122.

COLAGROSSI, A., SOUTO-IGLESIAS, A., ANTUONO, M. & MARRONE, S. 2013 Smoothed-particle-hydrodynamics modeling of dissipation mechanisms in gravity waves. *Phys. Rev. E* **87**, 023302.

DAIRAY, T., LAMBALLAIS, E., LAIZET, S. & VASSILICOS, J.C. 2017 Numerical dissipation vs. subgrid-scale modelling for large eddy simulation. *J. Comput. Phys.* **337**, 252–274.

DAUCH, T.F., RAPP, T., CHAUSSONNET, G., BRAUN, S., KELLER, M.C., KADEN, J., KOCH, R., DACHSBACHER, C. & BAUER, H.-J. 2018 Highly efficient computation of finite-time Lyapunov exponents (FTLE) on GPUs based on three-dimensional SPH datasets. *Comput. Fluids* **175**, 129–141.

DEHNEN, W. & ALY, H. 2012 Improving convergence in smoothed particle hydrodynamics simulations without pairing instability. *Mon. Not. R. Astron. Soc.* **425**, 1068–1082.

DI MASCIO, A., ANTUONO, M., COLAGROSSI, A. & MARRONE, S. 2017 Smoothed particle hydrodynamics method from a large eddy simulation perspective. *Phys. Fluids* **29**, 035102.

DRIKAKIS, D., FUREBY, C., GRINSTEIN, F.F. & YOUNGS, D. 2007 Simulation of transition and turbulence decay in the Taylor–Green vortex. *J. Turbul.* **8**, N20.

DU, Q. & TIAN, X. 2020 Mathematics of smoothed particle hydrodynamics: a study via nonlocal Stokes equations. *Foundations Comput. Maths* **20**, 801–826.

DURRAN, D., WEYN, J.A. & MENCHACA, M.Q. 2017 Practical considerations for computing dimensional spectra from gridded data. *Mon. Weath. Rev.* **145**, 3901–3910.

EIRÍS, A., RAMÍREZ, L., COUCEIRO, I., FERNÁNDEZ-FIDALGO, J., PARÍS, J. & NOGUEIRA, X. 2023 MLS-SPH-ALE: a review of meshless-FV methods and a unifying formulation for particle discretizations. *Arch. Comput. Meth. Engng* **30**, 4959–4981.

ELLERO, M., ESPAÑOL, P. & ADAMS, N.A. 2010 Implicit atomistic viscosities in smoothed particle hydrodynamics. *Phys. Rev. E* **82**, 046702.

EYINK, G. 2024 Onsager's ideal turbulence theory. *J. Fluid Mech.* **988**, P1.

EYINK, G.L. & DRIVAS, T.D. 2018 Cascades and dissipative anomalies in compressible fluid turbulence. *Phys. Rev. X* **8**, 011022.

FEHN, N., KRONBICHLER, M., MUNCH, P. & WALL, W.A. 2022 Numerical evidence of anomalous energy dissipation in incompressible Euler flows: towards grid-converged results for the inviscid Taylor–Green problem. *J. Fluid Mech.* **932**, A40.

FRONTIERE, N., RASKIN, C.D. & OWEN, J.M. 2017 CRKSPH – a conservative reproducing kernel smoothed particle hydrodynamics scheme. *J. Comput. Phys.* **332**, 160–209.

GERMANO, M. 1992 Turbulence: the filtering approach. *J. Fluid Mech.* **238**, 325–336.

GHOSAL, S. 1996 An analysis of numerical errors in large-eddy simulations of turbulence. *J. Comput. Phys.* **125** (1), 187–206.

GINGOLD, R.A. & MONAGHAN, J.J. 1977 Smoothed particle hydrodynamics: theory and application to non-spherical stars. *Mon. Not. R. Astron. Soc.* **181**, 375–389.

GRINSTEIN, F.F., MARGOLIN, L.G. & RIDER, W.J. 2007 *Implicit Large Eddy Simulation: Computing Turbulent Fluid Dynamics*. Cambridge University Press.

HALLER, G. 2015 Lagrangian coherent structures. *Annu. Rev. Fluid Mech.* **47**, 137–162.

HARDY, R.J. 1982 Formulas for determining local properties in molecular-dynamics simulations: shock waves. *J. Chem. Phys.* **76**, 622–628.

HEISENBERG, W. 1948 Zur statistischen theorie der turbulenz. *Z. Phys.* **124**, 628–657.

HOPKINS, P.F. 2015 A new class of accurate, mesh-free hydrodynamic simulation methods. *Mon. Not. R. Astron. Soc.* **450**, 53.

HOPKINS, P.F. 2016 Anisotropic diffusion in mesh-free numerical magnetohydrodynamics. *Mon. Not. R. Astron. Soc.* **466** (3), 3387–3405.

IRVING, J.H. & KIRKWOOD, J.G. 1950 The statistical mechanical theory of transport processes. IV. The equations of hydrodynamics. *J. Chem. Phys.* **18** (6), 817–829.

JAKOBSEN, H.A. 2014 *Chemical Reactor Modeling: Multiphase Reactive Flows*. Springer.

KING, J.R.C., LIND, S.J., ROGERS, B.D., STANSBY, P.K. & VACONDIO, R. 2023 Large eddy simulations of bubbly flows and breaking waves with smoothed particle hydrodynamics. *J. Fluid Mech.* **972**, A24.

KOLMOGOROV, A.N. 1941 The local structure of turbulence in incompressible viscous fluid for very large Reynolds numbers. *Dokl. Akad. Nauk SSSR* **30**, 4.

KÜCHLER, C., BEWLEY, G.P. & BODENSCHATZ, E. 2023 Universal velocity statistics in decaying turbulence. *Phys. Rev. Lett.* **131**, 024001.

KURGANOV, A. & TADMOR, E. 2000 New high-resolution central schemes for nonlinear conservation laws and convection–diffusion equations. *J. Comput. Phys.* **160** (1), 241–282.

LAI, X., LI, S., YAN, J., LIU, L. & ZHANG, A.-M. 2022 Multiphase large-eddy simulations of human cough jet development and expiratory droplet dispersion. *J. Fluid Mech.* **942**, A12.

LAIZET, S. & LI, N. 2011 Incompact3d: a powerful tool to tackle turbulence problems with up to $O(10^5)$ computational cores. *Intl J. Numer. Meth. Fluids* **67** (11), 1735–1757.

LIND, S.J., ROGERS, B.D. & STANSBY, P.K. 2020 Review of smoothed particle hydrodynamics: towards converged Lagrangian flow modelling. *Proc. R. Soc. Lond. A* **476**, 20190801.

LIND, S.J. & STANSBY, P.K. 2016 High-order Eulerian incompressible smoothed particle hydrodynamics with transition to Lagrangian free-surface motion. *J. Comput. Phys.* **326**, 290–311.

LIND, S.J., XU, R., STANSBY, P.K. & ROGERS, B.D. 2012 Incompressible smoothed particle hydrodynamics for free-surface flows: a generalised diffusion-based algorithm for stability and validations for impulsive flows and propagating waves. *J. Comput. Phys.* **231** (4), 1499–1523.

LUCY, L.B. 1977 A numerical approach to the testing of the fission hypothesis. *Astron. J.* **82**, 1013–1024.

LUND, T.S. 2003 The use of explicit filters in large eddy simulation. *Comput. Maths Applics.* **46** (4), 603–616.

MANSFIELD, J.R., KNIO, O.M. & MENEVEAU, C. 1998 A dynamic LES scheme for the vorticity transport equation: formulation and *a priori* tests. *J. Comput. Phys.* **145** (2), 693–730.

MANSFIELD, J.R., KNIO, O.M. & MENEVEAU, C. 1999 Dynamic LES of colliding vortex rings using a 3D vortex method. *J. Comput. Phys.* **152** (1), 305–345.

MARRONE, S., ANTUONO, M., COLAGROSSI, A., COLICCHIO, G., LE TOUZÉ, D. & GRAZIANI, G. 2011 δ-SPH model for simulating violent impact flows. *Comput. Meth. Appl. Mech. Engng* **200** (13), 1526–1542.

MERINGOLO, D.D., LAURIA, A., ARISTODEMO, F. & FILIANOTI, P.F. 2023 Large eddy simulation within the smoothed particle hydrodynamics: applications to multiphase flows. *Phys. Fluids* **35** (6), 063312.

MONAGHAN, J.J. 2012 Smoothed particle hydrodynamics and its diverse applications. *Annu. Rev. Fluid Mech.* **44**, 323–346.

MOSER, R.D., HAERING, S.W. & YALLA, G.R. 2021 Statistical properties of subgrid-scale turbulence models. *Annu. Rev. Fluid Mech.* **53**, 255–286.

MOURA, R.C., MENGALDO, G., PEIRÓ, J. & SHERWIN, S.J. 2017 On the eddy-resolving capability of high-order discontinuous Galerkin approaches to implicit LES / under-resolved DNS of Euler turbulence. *J. Comput. Phys.* **330**, 615–623.

NICOUD, F., TODA, H.B., CABRIT, O., BOSE, S. & LEE, J. 2011 Using singular values to build a subgrid-scale model for large eddy simulations. *Phys. Fluids* **23**, 085106.

OBUKHOV, A.M. 1941 On the distribution of energy in the spectrum of turbulent flow. *Dokl. Akad. Nauk SSSR* **32**, 22–24.

OGER, G., MARRONE, S., LE TOUZÉ, D. & DE LEFFE, M. 2016 SPH accuracy improvement through the combination of a quasi-Lagrangian shifting transport velocity and consistent ALE formalisms. *J. Comput. Phys.* **313**, 76–98.

OKRASCHEVSKI, M. 2024 Über den Zusammenhang von large eddy simulation und smoothed particle hydrodynamics. PhD thesis, Karlsruher Institut für Technologie (KIT), Karlsruhe, Germany.

OKRASCHEVSKI, M., BUERKLE, N., KOCH, R. & BAUER, H.-J. 2021*a* Implicit molecular stresses in weakly compressible particle-based discretization methods for fluid flow. *Phys. Rev. E* **103**, 033304.

OKRASCHEVSKI, M., BUERKLE, N., KOCH, R. & BAUER, H.-J. 2022 Smoothed particle hydrodynamics physically reconsidered: the relation to explicit large eddy simulation and the issue of particle duality. *Phys. Fluids* **34** (11), 115108.

OKRASCHEVSKI, M., HOFFMANN, S., STICHLING, K., KOCH, R. & BAUER, H.-J. 2021*b* Fluid dynamics beyond the continuum: a physical perspective on large-eddy simulation. *Phys. Rev. Fluids* **6**, L102601.

ONSAGER, L. 1945 The distribution of energy in turbulence. *Phys. Rev.* **68**, 281.

PANUELOS, J., WADSLEY, J. & KEVLAHAN, N. 2020 Low shear diffusion central schemes for particle methods. *J. Comput. Phys.* **414**, 109454.

PARK, N., YOO, J.Y. & CHOI, H. 2004 Toward improved consistency of *a priori* tests with *a posteriori* tests in large eddy simulation. *Phys. Fluids* **17** (1), 015103.

PEREIRA, F.S., GRINSTEIN, F.F., ISRAEL, D.M., RAUENZAHN, R. & GIRIMAJI, S.S. 2021 Modeling and simulation of transitional Taylor–Green vortex flow with partially averaged Navier–Stokes equations. *Phys. Rev. Fluids* **6**, 054611.

POSCH, H.A., HOOVER, W.G. & KUM, O. 1995 Steady-state shear flows via nonequilibrium molecular dynamics and smooth-particle applied mechanics. *Phys. Rev. E* **52**, 1711–1720.

PRICE, D.J. 2012 Smoothed particle hydrodynamics and magnetohydrodynamics. *J. Comput. Phys.* **231**, 759–794.

RENNEHAN, D. 2021 Mixing matters. *Mon. Not. R. Astron. Soc.* **506**, 2836–2852.

REYNOLDS, O. 1895 IV. On the dynamical theory of incompressible viscous fluids and the determination of the criterion. *Phil. Trans. R. Soc. Lond. A* **186**, 123–164.

SCHMITT, F.G. 2007 About Boussinesq's turbulent viscosity hypothesis: historical remarks and a direct evaluation of its validity. *C. R. Méc.* **335**, 617–627.

SHADLOO, M.S., OGER, G. & LE TOUZÉ, D. 2016 Smoothed particle hydrodynamics method for fluid flows, towards industrial applications: motivations, current state, and challenges. *Comput. Fluids* **136**, 11–34.

SIGALOTTI, L., KLAPP, J. & GESTEIRA, M. 2021 The mathematics of smoothed particle hydrodynamics (SPH) consistency. *Frontiers Appl. Maths Stat.* **7**. Available at: https://www.frontiersin.org/journals/applied-mathematics-and-statistics/articles/10.3389/fams.2021.797455/full.

SILVIS, M.H., REMMERSWAAL, R.A. & VERSTAPPEN, R. 2017 Physical consistency of subgrid-scale models for large-eddy simulation of incompressible turbulent flows. *Phys. Fluids* **29** (1), 015105.

SKRBEK, L. & STALP, S.R. 2000 On the decay of homogeneous isotropic turbulence. *Phys. Fluids* **12** (8), 1997–2019.

SPRINGEL, V. 2010 Smoothed particle hydrodynamics in astrophysics. *Annu. Rev. Astron. Astrophys.* **48**, 391–430.

TAYLOR, G.I. & GREEN, A.E. 1937 Mechanism of the production of small eddies from large ones. *Phil. Trans. R. Soc. Lond. A* **158**, 499–521.

TIAN, Y., WOODWARD, M., STEPANOV, M., FRYER, C., HYETT, C., LIVESCU, D. & CHERTKOV, M. 2023 Lagrangian large eddy simulations via physics-informed machine learning. *Proc. Natl Acad. Sci. USA* **120** (34), e2213638120.

VIGNJEVIC, R., DEVUYST, T. & CAMPBELL, J. 2021 The nonlocal, local and mixed forms of the SPH method. *Comput. Meth. Appl. Mech. Engng* **387**, 114164.

VILA, J.P. 1999 On particle weighted methods and smooth particle hydrodynamics. *Math. Models Meth. Appl. Sci.* **09** (2), 161–209.

VITTOZ, L., OGER, G., DE LEFFE, M. & LE TOUZÉ, D. 2019 Comparisons of weakly-compressible and truly incompressible approaches for viscous flow into a high-order Cartesian-grid finite volume framework. *J. Comput. Phys. X* **1**, 100015.

VOGELSBERGER, M., SIJACKI, D., KEREŠ, D., SPRINGEL, V. & HERNQUIST, L. 2012 Moving mesh cosmology: numerical techniques and global statistics. *Mon. Not. R. Astron. Soc.* **425** (4), 3024–3057.

VOLPIANI, P.S. 2024 A comprehensive study about implicit/explicit large-eddy simulations with implicit/explicit filtering. *Flow Turbul. Combust.* **113**, 891–922.

VREMAN, B., GEURTS, B. & KUERTEN, H. 1994 Realizability conditions for the turbulent stress tensor in large-eddy simulation. *J. Fluid Mech.* **278**, 351–362.

WOODWARD, M., TIAN, Y., HYETT, C., FRYER, C., STEPANOV, M., LIVESCU, D. & CHERTKOV, M. 2023 Physics-informed machine learning with smoothed particle hydrodynamics: hierarchy of reduced Lagrangian models of turbulence. *Phys. Rev. Fluids* **8**, 054602.

XU, R., STANSBY, P. & LAURENCE, D. 2009 Accuracy and stability in incompressible SPH (ISPH) based on the projection method and a new approach. *J. Comput. Phys.* **228** (18), 6703–6725.

YAO, W.-W., ZHOU, X.-P. & QIAN, Q.-H. 2022 From statistical mechanics to nonlocal theory. *Acta Mechanica* **233**, 869–887.

YE, T., PAN, D., HUANG, C. & LIU, M. 2019 Smoothed particle hydrodynamics (SPH) for complex fluid flows: recent developments in methodology and applications. *Phys. Fluids* **31**, 011301.

ZHU, Q., HERNQUIST, L. & LI, Y. 2015 Numerical convergence in smoothed particle hydrodynamics. *Astrophys. J.* **800**, 6.